Projecting Global Mercury Emissions and Deposition Under the Shared Socioeconomic Pathways

Benjamin M. Geyman[1], David G. Streets[1], Colin P. Thackray,[1] Christine L. Olson[2], Kevin Schaefer[2], and Elsie M. Sunderland[1,3]

[1] Harvard John A. Paulson School of Engineering and Applied Sciences, Cambridge, MA 01238, USA.
[2] National Snow and Ice Data Center, Cooperative Institute for Research in Environmental Sciences, University of Colorado Boulder, Boulder, CO, USA.
[3] Department of Environmental Health, Harvard School of Public Health, Boston, Massachusetts 02115, USA.

Corresponding author: Benjamin Geyman (bgeyman@fas.harvard.edu)

Key Points:

- Future (2010-2300) anthropogenic Hg releases to air, land and water (0.7-1.7 Tg) are similar to historical (1510-2010) releases (1.1-2.8 Tg)
- Cumulative anthropogenic Hg emissions to air (2010-2300) vary by a factor of two across scenarios (110-230 Gg)
- Deposition declines from near-term reductions in anthropogenic Hg emissions are amplified by reductions in re-emissions from land and ocean

Abstract

Mercury (Hg) is a naturally occurring element that has been greatly enriched in the environment by activities like mining and fossil fuel combustion. Despite commonalities in some CO_2 and Hg emission sources, the implications of long-range climate scenarios for anthropogenic Hg emissions have yet to be explored. Here, we present comprehensive projections of anthropogenic Hg emissions (2020-2300) and evaluate impacts on global atmospheric Hg deposition. Projections are based on four shared socioeconomic pathway (SSP) narratives ranging from sustainable reductions in resource and energy intensity to rapid economic growth driven by abundant fossil fuel exploitation. There is a greater than two-fold difference in cumulative anthropogenic Hg emissions between the lower-bound (110 Gg) and upper-bound (230 Gg) scenarios. Hg releases to land and water are approximately six times those of direct emissions to air (600-1470 Gg). At their peak, anthropogenic Hg emissions reach 2200-2600 Mg a^{-1} sometime between 2010 (baseline) and 2030, depending on the SSP scenario. Coal combustion is the largest determinant of differences in Hg emissions among scenarios. Decoupling of Hg and CO_2 emissions sources occurs under low- to mid-range scenarios, though contributions from artisanal and small-scale gold mining remain uncertain. A projected future shift in speciation of Hg emissions toward lower gaseous elemental Hg (Hg^0) and higher divalent Hg (Hg^{II}) will result in a higher fraction of locally-sourced Hg deposition. Projected re-emissions of previously deposited anthropogenic Hg follow a similar temporal trajectory to primary emissions, amplifying benefits of primary Hg emissions reductions under the most stringent mitigation scenarios.

Plain Language Summary

Mercury is a global pollutant that is emitted alongside greenhouse gases like carbon dioxide (CO_2) when fossil fuels such as coal are burned. Researchers have projected how emissions of greenhouse gases and climate are likely to change in the future, but relatively little is known about future Hg releases. Here, we project future Hg emissions between 2020 and 2300 using growth scenarios developed by climate change researchers. Under low emission scenarios, Hg emissions are projected to peak between 2010 and 2030. Under the high emission scenario, Hg releases continue near present-day levels until after 2060, and decline more slowly than other scenarios thereafter. Large variability in projected releases (cumulatively a two-fold difference) is apparent across the low and high scenarios. Globally, the intensity of coal combustion and how quickly it is phased out is the largest driver of future Hg releases. We then use global models to simulate future atmospheric Hg deposition, identifying multiple factors responsible for changing deposition patterns and amounts. We find there is a penalty for delaying reductions in Hg emissions because of increased reemissions from the land and ocean in the future. This work emphasizes the benefits of near-term stringent global reductions in anthropogenic Hg releases.

1 Introduction

Mercury (Hg) is a naturally occurring element, but human activities such as mining and fossil-fuel combustion have released approximately 1.5 Tg of Hg from stable geologic reservoirs to the atmosphere, land, and water over the past 500 years (1510-2010) (Streets et al., 2019a). This has significantly altered the natural biogeochemical Hg cycle (Geyman et al., 2023; Streets et al., 2019a) and adversely affected the health of exposed humans and wildlife (Basu et al., 2023). Reemission of anthropogenic Hg from terrestrial and aquatic ecosystems extends its lifetime in the biosphere (referred to as "legacy Hg"). Past work has quantified the impacts of historical emissions and legacy Hg cycling on the global Hg cycle (Amos et al., 2013; Angot et al., 2018; Guerrero & Schneider, 2023; Nriagu, 1994). However, estimates of future anthropogenic Hg emissions based on the most recent future growth scenarios adopted by the Intergovernmental Panel on Climate Change (IPCC) and their drivers are not presently available (O'Neill et al., 2016), limiting our ability to project future scenarios of Hg pollution.

Shared Socioeconomic Pathways (SSPs) and associated emission scenarios offer unified narratives ranging from sustainable development to fossil fuel-driven growth (O'Neill et al., 2016, 2017). They provide a framework for bounding development and greenhouse gas trajectories extending to the year 2300 (Meinshausen et al., 2020). However, these narratives do not explicitly address Hg emissions or the technological transformations underpinning future changes in Hg emission intensity. We fill this gap by developing a methodology for projecting time-dependent change in activity-specific Hg emission factors. This approach is built upon detailed parameterizations developed for historical emission inventories (Streets et al., 2011, 2019a), which facilitates intercomparison of past and future emissions.

Anthropogenic Hg is released to the atmosphere in both the elemental (Hg^0) and oxidized (Hg^{II}) forms. Hg^{II} has an atmospheric lifetime against deposition of a few days (Corbitt et al., 2011), while the lifetime of Hg^0 is greater than one year (Horowitz et al., 2017; Shah et al., 2021). Previous studies projected Hg deposition in 2035 and 2050 based on anthropogenic Hg emissions estimated from older IPCC Special Report on Emission Scenarios (SRES) and

independent estimates (Corbitt et al., 2011; Pacyna et al., 2016; Streets et al., 2009). Results suggested future increases in Hg^{II} emissions relative to Hg^0 are likely to increase the proportion of regional Hg deposition from emitting countries. The SRES emission trajectories ranged from a best-case scenario that showed relatively flat anthropogenic Hg emissions between 2006 and 2050, to a scenario characterized by higher energy and economic growth (A1B) that approximately doubled 2006 emissions levels (Streets et al., 2009). Results from Pacyna et al. (2016) ranged from a slight increase under a current policy scenario to -85% under a maximum feasible reduction case. However, these past studies did not consider future changes in marine and terrestrial Hg reservoirs that affect reemission of Hg^0 (Amos et al., 2013, 2014). This is important because terrestrial and marine Hg^0 evasion are thought to account for large fractions of the atmospheric Hg undergoing contemporary and future deposition (e.g., ~60% of 2050 deposition to the contiguous United States) (Corbitt et al., 2011).

The main objective of this work was to better understand how future anthropogenic Hg emissions and deposition vary among the most recent socioeconomic development pathways used by the IPCC. To do this, we developed new decadal projections of primary anthropogenic Hg emissions for the years 2020-2300 based on four distinct SSPs spanning a wide range of radiative forcings. Using a suite of global modeling tools, we quantified how changes in primary Hg emissions and re-emissions from terrestrial and marine ecosystems affect regional magnitudes and global patterns in atmospheric deposition. This work provides insights into how different fossil fuel use scenarios are likely to affect global Hg burdens and the potential effects of different pollution control efforts.

2 Methods

2.1 Description of Development Narratives (SSP Scenarios)

Forecasts of future anthropogenic Hg emissions were developed in accordance with the scenarios used in Phase 6 of the Coupled Model Intercomparison Project (CMIP6), organized under the auspices of the IPCC (O'Neill et al., 2016). The scenarios were based on a framework combining narratives of global development with emissions and climate projections from integrated assessment and climate models (O'Neill et al., 2016). The first component, the SSPs, are comprised of five distinct narratives describing alternative courses of societal development, as well as quantitative descriptions of population, economic growth, and urbanization (Dellink et al., 2017; Jiang & O'Neill, 2017; Kc & Lutz, 2017). The SSPs were elaborated using integrated assessment models (IAMs) to provide quantitative descriptions of energy use, greenhouse gas emissions, and land-use change (Riahi et al., 2017).

For each SSP narrative, multiple IAM trajectories were defined to describe both a baseline scenario, which assumes no additional climate policies or climate change impacts, and mitigation scenarios, in which further policies are adopted. SSP narratives can be combined with different climate forcing pathways to describe the physical response of the climate system. The climate forcing is defined according to the long-term global average radiative forcing (W m^{-2}; Myhre et al., 2013). Following convention, the scenarios used in this work are written as: $SSP_{x\text{-}y}$, where x is the SSP and y is the radiative forcing pathway (W m^{-2}) (O'Neill et al., 2016). Throughout the rest of this work, scenarios will be referred by their specific name (e.g., SSP1-2.6) or collectively as "SSPs."

For this work, we adopted the three major scenarios that were initially chosen for long-term extensions (LTE) to 2300 under CMIP6 (O'Neill et al., 2016), namely, SSPs 1-2.6, 5-3.4, and 5-8.5. Scenario SSP1-2.6 is a lower-bound on future emissions, reflecting strong emphasis on sustainability and intensive control of climate-forcing agents; SSP5-3.4 is known as the "*overshoot*" scenario and reflects short-term growth in fossil-fuel use and minimal consideration of climate control measures until 2040 followed by aggressive mitigation thereafter; SSP5-8.5 is an upper bound on emissions, in which fossil-fuel use continues with little consideration of climate mitigation or transition to clean technologies. Subsequently, Meinshausen et al. (2020) extended additional scenarios to beyond 2300, so we added a fourth scenario to our projections, the so-called "*middle-of-the-road*" scenario, SSP2-4.5 (Fricko et al., 2017).

The detailed raw activity data that are used in this work to characterize Hg emissions under these four scenarios out to 2100 follow the work of Rao et al. (2017), with LTE from 2100 to 2300 following the work of Meinshausen et al. (2020). The Hg emissions forecasts reported in this work map the trajectories of CO_2 forecasts contained in the previously mentioned publications and the emissions of other species as described in subsequent studies (Gidden et al., 2019; Lund et al., 2019; Turnock et al., 2020). However, this work contains the first reported projections of Hg emissions under CMIP6 scenarios.

The SSP scenarios were used primarily to project fossil-fuel use (coal and oil), the manufacture and use of refined industrial products, and economic parameters. However, there are no specific variables from which to calculate the extraction and production of raw materials and basic products because these are not directly relevant to emissions of greenhouse gases. However, they are very important as sources of mercury. Thus, for 21st century production of these materials, we used forecasts specifically generated by industry models, as follows: copper, zinc, and lead (Sverdrup et al., 2019); iron (Morfeldt et al., 2015); mercury (Sverdrup & Olafsdottir, 2020); and gold (Sverdrup et al., 2012); as well as the basic industrial products steel (Morfeldt et al., 2015) and cement (Zhang et al., 2018). The work of Watari et al. (2020, 2021) was valuable in guiding the pathways of metals extraction and use to the end of the century.

2.2 Mercury Emission Calculation

Mercury emissions under a future climate scenario (*f*) were calculated using Equation (1):

$$E_{t,r,s,f} = E_{2010,r,s} \times \left(\frac{A_{t,r,s,f}}{A_{2010,r,s,f}}\right) \times \left(\frac{EF_{t,r,s,f}}{EF_{2010,r,s,f}}\right), \#(1)$$

where E = emissions (Mg a^{-1}); t = decadal future year, r = world region, s = source type; A = activity level (in various units); and EF = emission factor (g per unit of activity).

Future Hg emissions were calculated by extrapolating 2010 base-year emissions, as reported in (Streets et al., 2017, 2019a), in accordance with the energy and activity forecasts for each of the four future scenarios (*f*) described in the previous section. Emissions were calculated for each decade between 2020 and 2300, though they reach zero between 2190 and 2250 across scenarios in accordance with SSP prescriptions. Emissions are zero beyond 2250 across all scenarios.

Emissions were calculated at world region level (r). The SSP forecasts were developed for five world regions: OECD, REF (Russia and Eastern Europe), ASIA, MAF (Middle East and Africa), and LAM (Latin America). This is a very coarse division of the world, which may be adequate for CO_2 studies, but is too aggregated for studies of Hg emissions and transport. In particular, the OECD region is spread across the globe, with contributions from Western Europe, North America, Australasia, and Japan. The prior Hg emission estimates for 2010 (Streets et al., 2019a, 2019b), upon which this work is based, were calculated for 17 world regions and subsequently aggregated to seven: North America (NAM), South America (SAM), Western Europe (EUR), the Former Soviet Union (FSU), Africa/Middle East (AFM), Asia (ASA), and Oceania (OCA). By examining 2010 Hg emissions in the world regions used in each of these two studies, a simple equivalence was determined and applied in this work, as follows: NAM = 0.5 OECD + 0.1 LAM; SAM = 0.9 LAM; EUR = 0.3 OECD; FSU = REF; AFM = MAF; ASA = ASIA + 0.05 OECD; and OCA = 0.15 OECD. Emissions at the global scale (GLO) are thus identical. Though this is less than an ideal solution—because of potential future differences in the rates of development among the countries comprising the coarse SSP regions—it is certainly an improvement over the five SSP regions from the perspective of estimating Hg transport and deposition.

The SSP scenarios contain more than 600 activity components (A), covering all aspects of future energy, industrial, and economic development. The prior 2010 Hg emission estimates were developed for 18 source types (s) (Streets et al., 2017). Because none of the SSP scenarios provide activity components that can be unequivocally associated with several of the Hg source types, emissions from 11 source types were projected individually in this work: mining (copper, zinc, lead, iron, mercury, gold, and artisanal gold), steel production, cement production, coal combustion, and oil combustion. Six other source types (municipal waste incineration, other waste combustion, electrical and measuring equipment, chemicals manufacturing, caustic soda production, and dental) were projected in aggregate. Silver mining was not included in this work because emissions from 2010 onwards are expected to be zero.

The change in activity levels in the future, A_t/A_{2010}, reflects the growth or shrinkage in activity for a particular source type, in a particular region, under a particular scenario. Some may grow, some may decline, depending on the influence of the world economy in general and the pressure of the climate change scenario. For example, coal combustion may increase under a lax climate scenario or decline under a stringent one. But A_t/A_{2010} only characterizes the change in the size of the source type, it says nothing about the transformation of it over the time period in question. New, high-performing technologies will undoubtedly replace older, low-performing ones; and the imposition of new emission control regulations may or may not force the use of add-on emission control technologies or even a complete change in production technology. All of these will influence Hg emissions. Except for Carbon Capture and Storage (CCS) and inferences from SO_2 emissions, the SSP scenarios say nothing about technology transformation that will influence Hg emissions. This, therefore, is the most challenging aspect of forecasting future Hg emissions. Our approach was to develop the ratio $EF_{t,r,s,f}/EF_{2010,r,s,f}$ as an indicator of how future emission rates will decline from their 2010 values. Note that this ratio is never greater than one (i.e., future emission rates are never higher in the future than in 2010 per unit of activity).

In previous work, we developed a methodology for estimating the time-development of emission factors for historical periods (pre-2010) using transformed normal distribution functions (Streets

et al., 2011). These region-specific functions were parameterized based on a detailed review of experimental measurements around the world, as illustrated in that paper for copper smelting. It was shown, for example, that the Hg emission rate for copper smelters pre-1900 was an uncontrolled value of 27.5 gHg/MgCu worldwide. After 1900, emission rates declined, along different pathways in different parts of the world, reaching values in 2010 ranging from a low of 0.60 gHg/MgCu in western Europe to a high of 11.6 gHg/MgCu in Africa.

The challenge in this work was to reasonably represent the continuation of historical *EF* trends out beyond 2010 in the absence of guidance from the SSP forecasts. In this work, we focused on the period 2010–2100, where technology transformation will have the biggest effect. For each of the 11 key source types mentioned above, we assumed that by 2100 the emission rates in every world region will have declined from their 2010 levels to the present-day emission rate of the lowest-emitting region. Thus, in the case of copper smelting, all regions emit at 0.60 gHg/MgCu by 2100, though the trajectories to reach it vary by region. This 2100 rate then continues for all years beyond 2100. Intermediate decadal years in *EF* were determined as linear trends.

For the purposes of atmospheric modeling, speciation of these future atmospheric Hg emissions into elemental Hg (Hg^0) and divalent Hg compounds (Hg^{II}) was determined in a similar way, by extrapolation of the speciation splits in each region in the year 2010. These range rather widely, from a high value of the Hg^0/Hg ratio of 0.88 in South America to a low of 0.25 in western Europe. This reflects the different emission characteristics of, for example, mining in South America and industrial manufacturing/well-controlled coal combustion in western Europe. As time goes on it can be expected that the Hg^0/Hg ratio will decline everywhere, as artisanal and small-scale mining techniques (with high Hg^0 emission rates) are retired, and industrial processes and combustion become increasingly well controlled, leading to conversion of elemental Hg to collectable, oxidized Hg compounds. In this work, we assumed that the 2010 ratios in high-emitting regions approach the western European level or the North American level (0.33) by 2100, eventually leveling out at a technology-limiting value of 0.2 everywhere. Slight variations were applied among the four scenarios to reflect anticipated patterns of future technology transformations.

Finally, future releases of Hg to land and water were estimated following the method of Streets et al. (2017, 2019a). In essence, this involves subtracting the air emissions from the total Hg contained in the raw material that is processed. It was not possible to determine *a priori* the fate of these releases by source type, technology level, or world region. Uncertainties in the few quantitative estimates that have been made and the vast quantity of unknown factors for sources in remote parts of the world essentially rule this out.

2.3 Global Atmospheric Hg Deposition

We used the GEOS-Chem global chemical transport model to simulate the atmospheric fate and deposition of mercury emissions under each emissions scenario. The model version (12.8) used here included detailed multi-phase oxidation of elemental Hg and gas-phase photolysis of oxidized Hg species from Shah et al. (2021). Simulations were run using 2014-2019 MERRA-2 meteorology (Gelaro et al., 2017) on a 2 × 2.5-degree horizontal grid with a 72-layer vertical domain extending through the top of the stratosphere. The first two years of each simulation

were used for initialization and the final three years were averaged for analysis to reduce the effects of meteorological variability on simulated deposition patterns.

We conducted 5-year simulations for each decade from 2020-2100 for each scenario in addition to a common baseline scenario for the 2010 emission year. We hold meteorology constant across decadal snapshots to isolate the effects of variation in future emissions. Emissions from the seven world regions were distributed onto a 0.25 × 0.25-degree grid based on the spatial distributions established in prior work (Steenhuisen & Wilson, 2019). Relative fractions of North American emissions from Canada, the United States, and Central America were scaled to reflect 2015 values reported in Streets et al. (2019b) for consistency with past work.

We constructed source-receptor functions to quantify changes in atmospheric Hg deposition resulting from shifts in terrestrial and oceanic Hg^0 evasion and for each anthropogenic emission region. Following Corbitt et al. (2011), we define each source-receptor function F_{ij} as:

$$F_{ij} = \frac{D_{ij}}{E_i} \#(2)$$

where D_{ij} is the total mercury deposition flux to receptor grid cell j from emissions in region i, and E_i is the magnitude of emissions from region i.

2.4 Global Biogeochemical Box Model (GBBM)

An updated version of the multi-compartment Global Biogeochemical Box Model (GBBM) developed by Amos et al. (2013; 2014) was used to simulate future shifts in atmospheric deposition from legacy mercury emissions (Text S1; Table S1-S2). The GBBM represents Hg cycling between the atmosphere, terrestrial biosphere (fast, slow, protected), ocean (surface, intermediate, deep), and removal by burial in marine sediment.

We added four new compartments to the GBBM that represent waste reservoirs (fast, slow, protected, and immobilized) to explicitly track the fate of the estimated 1.13 Tg Hg released by humans to land and water from 1510-2010 (Streets et al., 2019a). These releases included tailings and waste from mining and metals production, chlor-alkali plants, and substantial contributions from Hg use in commercial products (Horowitz et al., 2014; Streets et al., 2011). In prior work, anthropogenic releases to land and water were added to soil compartments of the GBBM (Streets et al., 2017). However, it is likely that the majority of such releases are sequestered at contaminated sites and do not have the same diffuse impacts on deposition as atmospheric sources (Guerrero & Schneider, 2023; Kocman et al., 2017). Therefore, we independently tracked land and water Hg releases. We parameterized re-emissions of Hg^0 and discharges of Hg^{II} to rivers from waste compartments using the same rate coefficients as for the fast, slow, and protected terrestrial Hg in the GBBM. Land and water Hg releases were partitioned into waste pools following the methods described in Streets et al. (2017) (Text S1).

We simulated the time-dependent fate of future anthropogenic Hg releases separately for each scenario. In each simulation, the model was initialized by calculating the steady state distribution of mercury among reservoirs under a constant geogenic Hg flux of 230 Mg a^{-1} from subaerial volcanism and 50 Mg a^{-1} from hydrothermal vents (Geyman et al., 2023). The model was then

forced with all-time (2000 BCE to 2010 CE) anthropogenic mercury releases from Streets et al. (2019) followed by emissions specified in each scenario from 2010-2300. Evaluation of model results for the year 2010 agree with the observational ranges for the atmospheric Hg reservoir, seawater concentrations, and atmospheric deposition enrichment factors (Table S3, Amos et al., 2015).

3 Results and Discussion

3.1 Future Emission Trends

3.1.1 Long-term perspective on anthropogenic Hg releases

Atmospheric Hg emissions are shown by region (Fig. 1; Table S4) and source sector (Table S5) for each of the four scenarios considered in this work. All primary Hg emissions are projected to be zero beyond 2250, consistent with SSP assumptions. Projected cumulative Hg releases to air, land, and water between 2010 and 2300 range from 709 Gg under SSP1-2.6, to 1710 Gg under SSP5-8.5. Projected anthropogenic emissions between 2010 and 2300 are comparable to cumulative historical emissions from 1510-2010 (1470 Gg) estimated in past work (Streets et al., 2019a), suggesting human impacts on the global Hg cycle will be sustained for millennia.

Global Hg emissions projected in this work for the year 2050 are substantially lower than similar forecasts made over a decade prior (2300-4900 Mg a^{-1}) using the IPCC SRES scenarios (Streets et al., 2009). Projected anthropogenic emission declines for the year 2050 under SSP1-2.6 (-1080 Mg a^{-1}) are similar to those projected for 2035 by Pacyna et al. (2016) under a scenario involving full implementation of policy commitments and plans made before 2016. Relative declines projected in this work are partially attributable to lower Hg emission factors from recently implemented Hg pollution controls (e.g., Zhang et al., 2023). Thus, lower future Hg emissions estimated in this work reflect progress made through global policy efforts in recent decades.

Across all scenarios, future land and water Hg releases follow qualitatively similar trajectories to atmospheric emissions. Land and water Hg releases grow as a fraction of total anthropogenic Hg releases in the future. By 2100, anthropogenic Hg releases to land and water are estimated to be 12 to 25 times greater than anthropogenic Hg emissions to air, compared to only 3.3-fold greater (7330 Mg a^{-1}) in 2010.

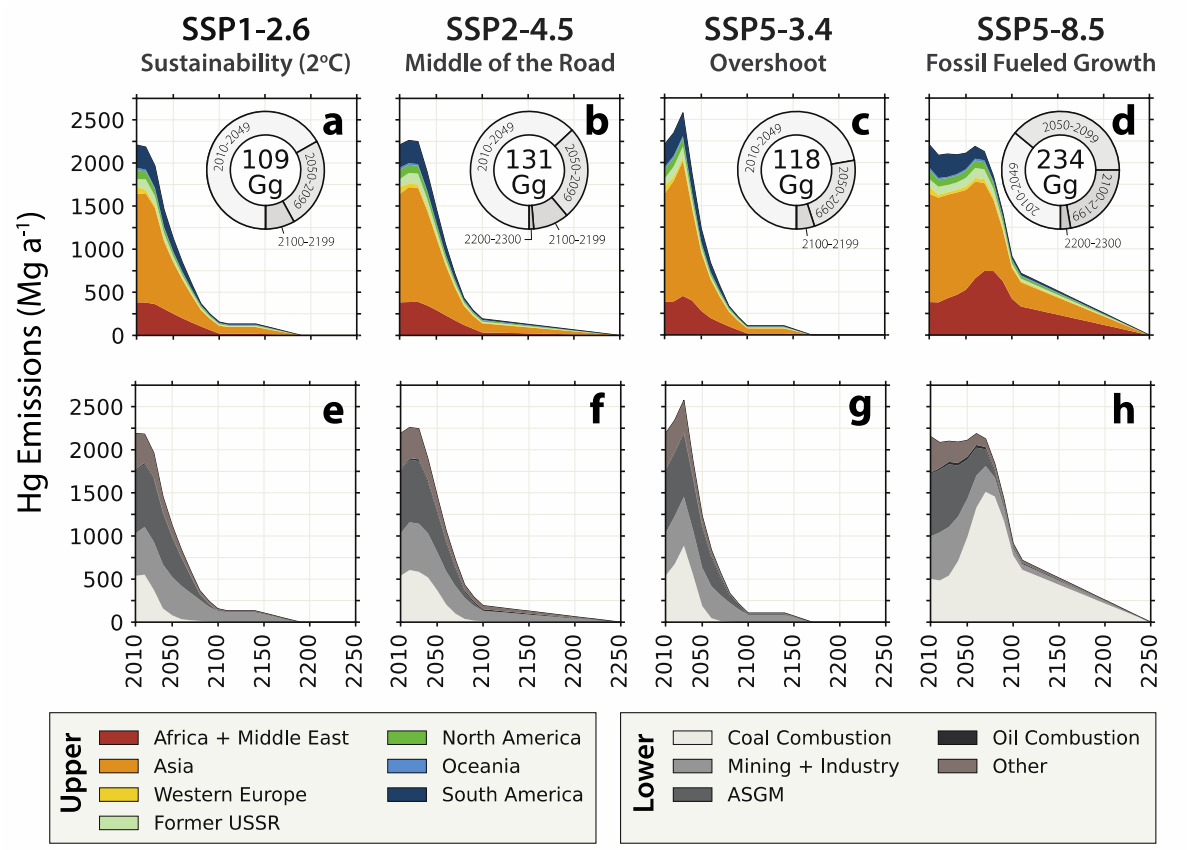

Figure 1. **Global anthropogenic mercury (Hg) emissions to air by world region and source sector.** Trajectories under each scenario are shown by world region in Panels (**a** – **d**). Inset pie charts show fractional emissions occurring during four "snapshot" time periods, arranged clockwise from the bottom: 2010-2049, 2050-2099, 2100-2200, 2200-2300. Cumulative emissions to air (Gg; 2010-2300) are shown in the center of each ring. Panels (**e** – **f**) provide a sector-specific breakdown of the same emission. ASGM = artisanal and small-scale gold mining.

3.1.2 Scenario-specific patterns in primary anthropogenic Hg releases

Among scenarios considered in this work, SSP1-2.6 is a lower-bound greenhouse gas emissions case, and it is known as the "2°C scenario." SSP1-2.6 is characterized by aggressive reductions in greenhouse gas emissions and a nameplate end-century radiative forcing of 2.6 W m^{-2} (Meinshausen et al., 2020). Projected future atmospheric Hg emissions decline continuously after 2010 (Fig. 1). In 2010, Asia was the largest regional contributor (1260 Mg a^{-1}; 57% of total) to global atmospheric emissions (2190 Mg a^{-1}). Under SSP1-2.6, a 93% reduction in global Hg emissions is projected (154 Mg a^{-1}) by the year 2100, and Asia remains the largest remaining regional emitter (91 Mg a^{-1}, 59%). Beyond 2100, emissions continue to decline at a slower pace and reach zero by 2190, in accordance with SSP assumptions.

SSP2-4.5 is a middle-of-the-road scenario that reflects moderate socioeconomic, energy, and climate mitigation changes and a continuation of growth and development trajectories following the status quo (Meinshausen et al., 2020). Relative to 2010, Hg emissions grow slightly until

2030 and then decline at a rate similar to SSP1-2.6 (Fig. 1). Hg emissions are 193 Mg a^{-1} by 2100, which is only 25% greater than SSP1-2.6 (Fig. 1). SSP2-4.5 is not nearly as close to the middle of the road for Hg emissions as it is for carbon emissions because it relies heavily on a switch from coal to natural gas as the primary energy supply under moderate climate mitigation efforts. This strategy results in continued greenhouse gas emissions and therefore results in middle of the road climate effects. However, natural gas combustion generates insignificant quantities of Hg, and so the trajectory is much lower. Hg emissions under SSP2-4.5 continue at a low level into the distant future, eventually reaching zero in 2250 following SSP assumptions (Fig. 1). Between 2010 and 2300, cumulative emissions to air are 131 Gg and cumulative emissions to land and water are 737 Gg under SSP2-4.5.

SSP5-3.4 is the overshoot case characterized by a delay in climate-change action until after 2030, leading to a major rise in Hg emissions between 2010 and 2030. Hg emissions are projected to rise to 2580 Mg a^{-1} by 2030, an increase of 17% over 2010 (Fig. 1). Much of that growth occurs in Asia. After 2030, emissions decline more precipitously than under the other three scenarios, reaching levels similar to SSP1-2.6 by 2060. Hg emissions fall to 107 Mg a^{-1} by 2100 and reach zero in the year 2170, which is earlier than SSP1-2.6. Under SSP5-3.4, cumulative emissions to air are projected to be 118 Gg. Compared to SSP1-2.6, cumulative emissions are heavily weighted toward the first few decades of the projection period. Cumulative emissions to land and water are 618 Gg.

SSP5-8.5 is the upper-bound case, characterized by continued fossil-fuel use and minimal consideration of environmental sustainability. Under this scenario, CO_2 concentrations are projected to reach levels greater than 2000 ppm by 2200 (Meinshausen et al., 2020). Such levels have not occurred on Earth since before the onset of the modern Antarctic glaciation over 40 Mya (Rae et al., 2021), and are associated with temperatures 3.3°C to 5.7°C higher in 2100 than during the early-industrial period (1850-1900) (IPCC, 2023). Emissions of Hg to air remain near present levels until after 2060 and then decline to 914 Mg a^{-1} (5-9 times the other scenarios) by the end of the 21st century. The dominant Hg emission regions are Asia, where emissions exceed 1000 Mg a^{-1} through 2070, and Africa and the Middle East, where emissions grow from 383 Mg a^{-1} in 2010 to 744 Mg a^{-1} in 2080. Emissions decline slowly beyond 2100, remaining at high levels into the 22nd century: 512 Mg a^{-1} in 2150 and 256 Mg a^{-1} in 2200 (Fig. 1). Emissions do not reach zero until 2250. Cumulative Hg releases (2010-2300) are 235 Gg to air and 1.47 Tg to land and water under SSP5-8.5.

Several indicators suggest that global anthropogenic Hg emissions are tracking below levels described in the overshoot scenario (SSP5-3.4) since 2010. While existing emission inventories report growth in global anthropogenic Hg emissions between 2010 and 2015 (Streets et al., 2019b), domestic policies have prompted widespread installation of air pollution control devices over the past decade in China (Zhang et al., 2023) and the United States (Dai et al., 2023). Trends in Hg^0 concentration and isotopic composition from long-term monitoring sites in China also show declines consistent with suggested reductions in regional anthropogenic emissions (Wu et al., 2023).

3.1.3 Decoupling of Hg emissions and radiative forcing under low coal use scenarios

Among source sectors in 2010, artisanal and small-scale gold mining (ASGM) was the largest global source of atmospheric emissions (727 Mg a^{-1}), followed by coal combustion (538 Mg a^{-1}) and mining and industry (491 Mg a^{-1}). Large-scale (rather than ASGM) gold production was the largest source of Hg released to land and water (1990 Mg a^{-1}), followed by ASGM (1090 Mg a^{-1}), electrical and measurement equipment (1010 Mg a^{-1}), chemicals manufacturing (860 Mg a^{-1}), and zinc smelting (670 Mg a^{-1}). Coal combustion accounted for a greater fraction of global atmospheric emissions (25%) in 2010 compared to land and water releases (5%, 370 Mg a^{-1}).

Differences in anthropogenic Hg emissions to air principally reflect differences in coal combustion across SSP scenarios. Hg emissions from coal combustion are projected to grow by 2.3 to 12.5% and peak in 2020 under SSPs 1-2.6 and 2-4.5 (Fig. 1). Near-term increases in Hg emissions from coal combustion reach levels 65% higher than 2010 under SSP5-3.4. Hg emissions decline thereafter for lower coal-use scenarios (SSPs 1-2.6, 2-4.5 and 5-3.4). By 2050, they fall to a fraction of 2010 levels (15% under SSP1-2.6 and 69% under SSP2-4.5) and reach zero before the end of the century. In contrast, coal combustion persists until 2250 under SSP5-8.5. Coal-related Hg emissions under SSP5-8.5 reach 990 Mg a^{-1} (96% higher than 2010) by 2070 and remain 44% higher than 2010 levels by the end of the century (Fig. 1).

Among lower coal-use scenarios, coal combustion is responsible for 16 Gg (SSP1-2.6) to 28 Gg (SSP2-45) of cumulative (2010-2300) Hg emissions to air. Cumulative Hg emissions to air from coal combustion are ~5 to 9-fold greater under SSP5-8.5 (139 Gg) than the other scenarios, and coal combustion comprises 59% of all emissions to air between 2010 and 2300 under SSP5-8.5.

Despite relative similarities in the phase-out of coal, SSPs 1-2.6, 2-4.5, and 5-3.4 show very different greenhouse gas emission trajectories. Such differences arise from rates of natural gas and oil combustion, as well as adoption of carbon capture and sequestration. These factors exert minimal direct influence on primary anthropogenic Hg emissions, though they produce disparate climate effects. For example, end-century surface temperatures simulated with the NASA GISS-E2.1 climate model are 1.8°C – 2.3°C higher than the preindustrial (1850-1880) mean under SSP1-2.6 compared to 2.7°C – 3.3°C under SSP2-4.5 (Nazarenko et al., 2022). The degree of warming will modulate future changes in Hg emissions from the natural biosphere (e.g., Krabbenhoft & Sunderland, 2013; Schaefer et al., 2020). Therefore, it is important to consider the consequences of human activity for both direct anthropogenic Hg releases and warming-driven changes in Hg cycling in the biosphere and ocean (e.g., Schaefer et al., 2020; Schartup et al., 2019).

3.1.4 Changes in Hg emission speciation favor local and regional deposition

The fraction of primary anthropogenic Hg emissions released to air as Hg^0 is projected to decline in the future (Fig. 2), with implications for transboundary pollution. For SSP1-2.6, the fraction of Hg^0 emitted by primary sources is projected to decline by 28% between 2010 and 2100. It stabilizes from 2100-2140, and then declines continuously thereafter. By 2180, the last decade with non-zero emissions for SSP1-2.6, Hg^0 is projected to make up just 20% of total anthropogenic Hg emissions to air (Fig. 2). Emission speciation under SSP5-3.4 broadly follows that of SSP1-2.6, with slightly higher Hg^0 fractions through 2100, and an accelerated decline between 2140 and 2160 from 31% Hg^0 to 20% Hg^0 (Fig. 2). Under SSP2-4.5, Hg^0 comprises a larger fraction of total Hg emissions to air than under SSPs 1-2.6 and 5-3.4, remaining around

55% until 2040 (Fig. 2). The Hg^0 fraction then exhibits a slow decline with overall emissions and reaches 22% by 2240 (Fig. 2). SSP5-8.5 consistently represents an upper bound for the Hg^0 fraction, increasing to 57% in 2060, followed by near-continuous declines to reach 22% by 2240. While trajectories vary across scenarios, greater fractions of Hg^{II} relative to Hg^0 in primary anthropogenic emissions are expected to produce future deposition patterns from primary emissions that increasingly reflect local and regional rather than global sources (Fig. S1).

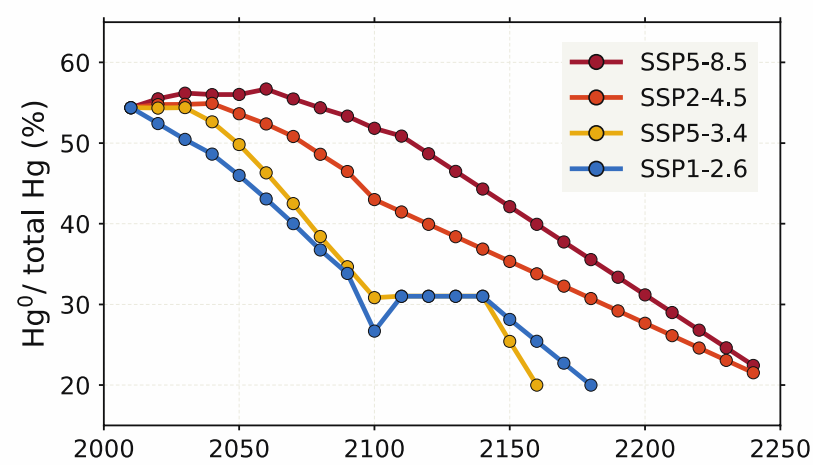

Figure 2. Decadal changes in the speciation of primary anthropogenic mercury (Hg) emissions to air. The percentage of total Hg emissions to air released as elemental Hg (Hg^0) is shown for each scenario and the remaining fraction consists of divalent mercury (Hg^{II}).

3.2. Future Deposition Patterns from Primary Anthropogenic Emissions

Modeled global Hg deposition to land increases by 22 Mg a^{-1} (0.9%) between 2010 and 2020 under SSP1-2.6 emissions. This reflects increases from both primary anthropogenic emissions (+8 Mg a^{-1}) and higher re-emissions from terrestrial and ocean surfaces due to increasing Hg reservoirs (+14 Mg a^{-1}) (Fig. S2). Modeled increases in regional Hg deposition occur during this period over all global regions except for Europe and North America (Fig. 3a; 4a). There, declines in deposition from primary anthropogenic sources exceed increases in deposition from growing global terrestrial and oceanic Hg reservoirs and subsequent re-emissions. From 2040 through the end of the century, declines in atmospheric Hg deposition are projected for all regions. By 2100, total atmospheric Hg deposition is projected to be less than half of 2010 levels (46%, 1120 Mg a^{-1}) (Fig. S2). The largest regional deposition declines are projected over Asia (–510 Mg a^{-1}; –73%) because it was the largest source region in 2010 (Fig. 3a).

Temporal patterns in atmospheric Hg deposition under SSP2-4.5 are qualitatively similar to those of SSP1-2.6, characterized by slight but regionally heterogeneous near-term increases that give way to continuous decreases. Relative to 2010, global deposition increases by 1.7% in 2020 and 1.6% in 2030. These increases occur over all regions except Europe, where declines are smaller than for SSP1-2.6 (–17% in 2020 and 2030) (Fig. 3b). By the end of the century, deposition to land is 1270 Mg a^{-1} lower than in 2010 (Fig. S2), with regional declines reaching 71% (–25 μg m^{-2} a^{-1}) in Asia (Fig. 3b).

Under SSP5-3.4, near-term deposition increases considerably, growing to 2690 Mg a^{-1} (+9%) in 2030 over land (Fig. S2). The greatest increases occur in Asia, where total Hg deposition reaches 41 μg m^{-2} a^{-1} (+18%) in 2030. Deposition grows by greater than 8% over all regions except Europe. After 2030, accelerated emission reductions relative to SSP1-2.6 result in comparable end-century deposition, which is 1340 Mg a^{-1} lower than in 2010 (Fig. S2).

Atmospheric deposition under SSP5-8.5 is much higher than the other scenarios through most of the century. However, 2020 deposition is the lowest of all scenarios, and 2030 deposition is lower than all scenarios other than SSP1-2.6 (Fig. S2). Growth in emissions from Africa and the Middle East, combined with sustained emissions elsewhere, produce increasing deposition over most regions from 2020 until 2070. Most notably, deposition to Africa and the Middle East reach levels 18% higher (+2.5 μg m^{-2} a^{-1}) by 2070 and remain above baseline levels through 2100 (Fig. 3d; Fig. S2). End-century total deposition to land is 650 Mg a^{-1} lower than in 2010.

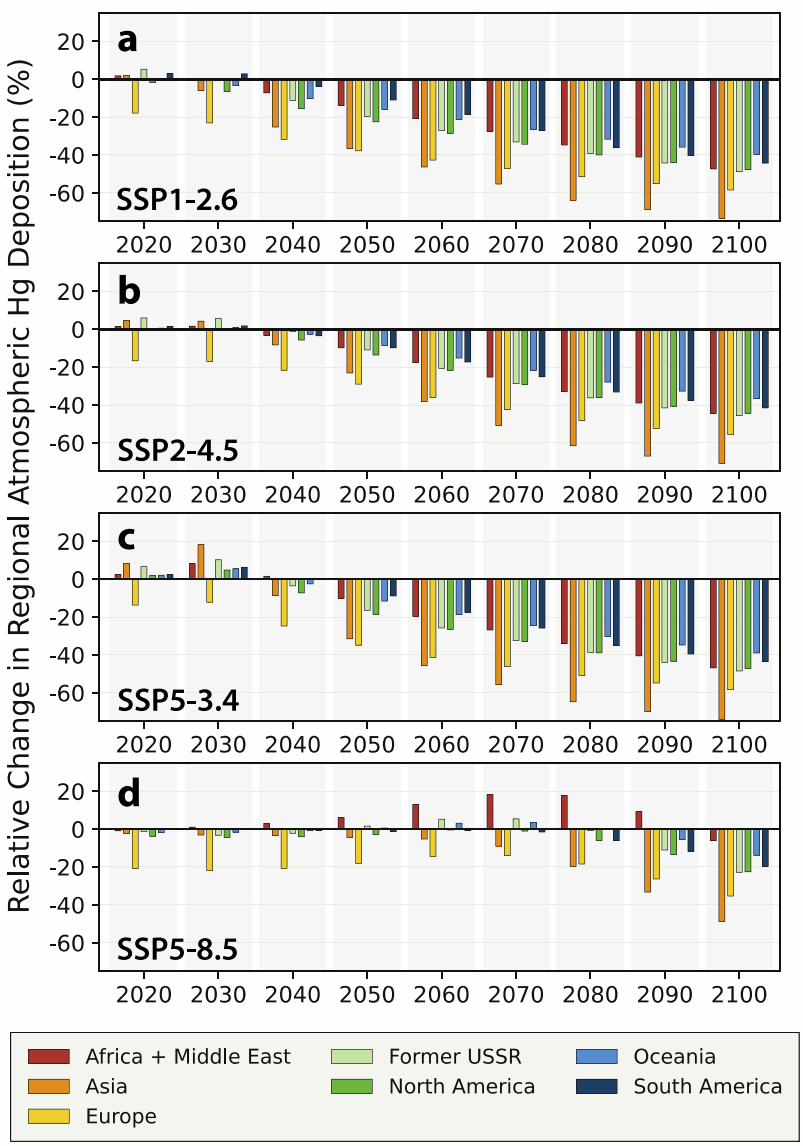

Figure 3. Relative changes in regional atmospheric mercury (Hg) deposition compared to 2010. Changes in atmospheric Hg deposition are shown by world region (represented by colored bars) for each decade from 2020 to 2100 (x-axis). Each subplot represents temporal trends under a different Shared Socioeconomic Pathway (SSP) scenario (O'Neill et al., 2016).

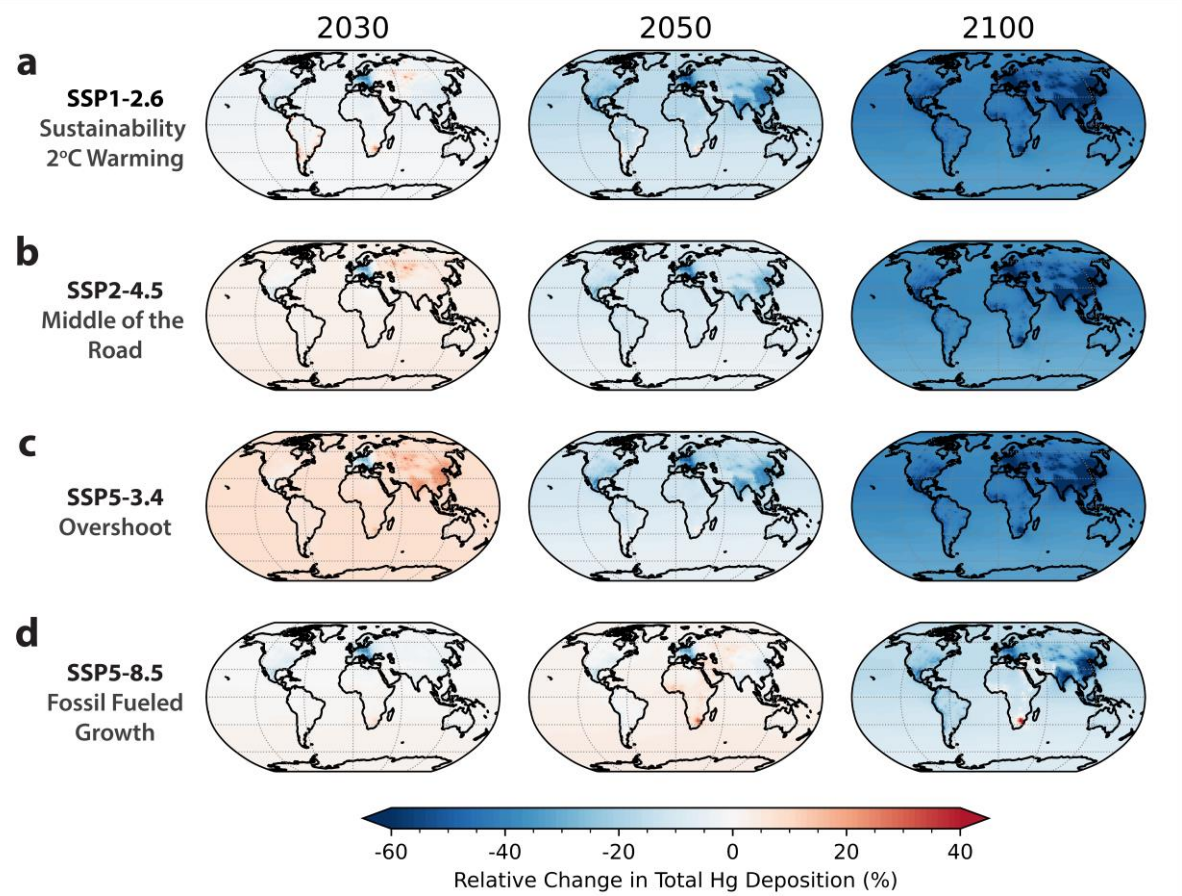

Figure 4. Trajectories of global atmospheric mercury (Hg) deposition. Panels represent fractional change in total deposition relative to the 2010 baseline by scenario (rows) for three time periods: 2030 (left), 2050 (center) and 2100 (right). Deposition is calculated as the sum of deposition from primary, legacy, and natural Hg emissions using the GEOS-Chem atmospheric mercury model (Shah et al., 2021) and the Global Biogeochemical Box Model (GBBM; Amos et al., 2013, 2014).

3.3 Implications for Legacy Hg Deposition from Terrestrial and Aquatic Emissions

Scenarios for deposition of legacy Hg vary among the four SSPs. Legacy deposition peaks before 2035 at levels 20 – 62 Mg a^{-1} higher than 2010 under SSPs 1-2.6, 2-4.5, and 5-3.4 (Fig. 5). Legacy deposition under SSP5-8.5 exhibits a larger and later peak, exceeding 2010 deposition by 66 Mg a^{-1} in 2071 (Fig. 5). By 2100, relative trends in legacy deposition are notably different, with declines of 330 – 380 Mg a^{-1} relative to 2010 for SSPs 1-2.6, 2-4.5 and 5-3.4, compared with a decline of 47 Mg a^{-1} for SSP5-8.5 (Fig. 5). These end-century declines in legacy emissions are responsible for 26 – 28% of total declines in atmospheric Hg deposition to land under SSPs 1-2.6, 2-4.5, and 5-3.4, compared to 7% for SSP5-8.5.

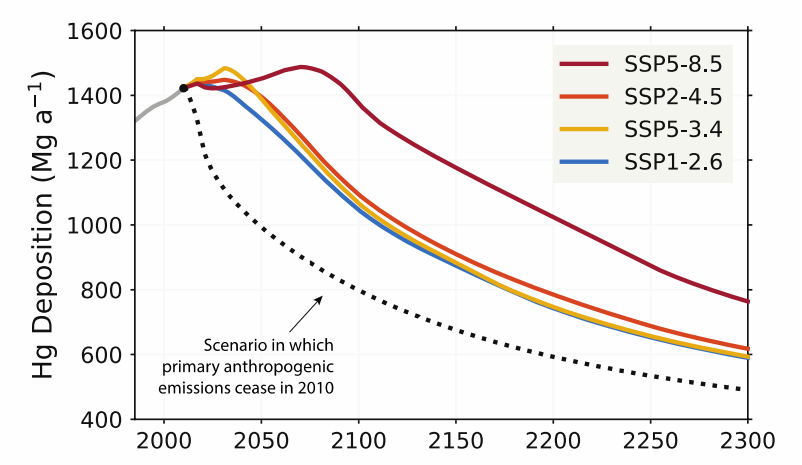

Figure 5. Mercury (Hg) deposition to land from legacy and natural emissions. Trajectories under future emissions (2010-2300) are shown for SSPs 1-2.6 (blue line), 2-4.5 (orange line), 5-3.4 (yellow line), and 5-8.5 (red line), in addition to a hypothetical scenario where primary anthropogenic emissions are zero after 2010 (dotted black line). Implications of future trajectories for upper ocean reservoirs are shown in Figure S4.

Comparing SSPs 1-2.6 and 5-3.4 provides insights into the consequences of delaying emission reductions. Cumulative emissions through 2100 are comparable for SSP1-2.6 (101 Gg) and SSP5-3.4 (112 Gg). Additionally, anthropogenic Hg emissions are lower in 2100 under SSP5-3.4 than SSP1-2.6 (107 Mg a^{-1} and 154 Mg a^{-1}). Higher deposition to anthropogenic receptor regions in 2100 under SSP5-3.4 reflects a legacy deposition penalty for the unrestrained growth of the first three decades of the century. Deposition from legacy emissions is 20 Mg higher in 2100 for SSP5-3.4 compared to SSP1-2.6, whereas deposition from primary anthropogenic emissions is 16 Mg lower. This example demonstrates the long-term benefits associated with near-term emissions mitigation, as discussed previously in Angot et al. (2018) and Amos et al. (2013).

By the end of the century, Hg re-emissions from the ocean and land will become relatively more important as sources of Hg deposition (Fig. S3), but deposition will not be evenly distributed by world region. Our source-receptor modeling suggests that South America receives the largest share of legacy Hg deposition on a per-area basis, receiving 23% higher deposition per unit of terrestrial emissions and 48% higher deposition per unit of ocean evasion than the area-weighted average of all world regions (Fig. 6). Such high rates of deposition over South America are driven by high rates of foliar uptake and wet deposition. In contrast, Oceania receives the lowest areal share of terrestrial emissions (73% of average), and the Former USSR receives the smallest areal share of Hg sourced from oceanic evasion (74% of average) (Fig. 6). Such low deposition is driven by the relative isolation of Oceania from terrestrial emissions and of the Former USSR from ocean emissions. These source-receptor relationships are subject to change in the future due to shifting patterns of historical anthropogenic Hg loading (e.g., Zolkos et al., 2022) and changing biogeochemical dynamics mediating deposition (e.g., Alexander & Mickley, 2015; Krabbenhoft & Sunderland, 2013; Yang et al., 2019).

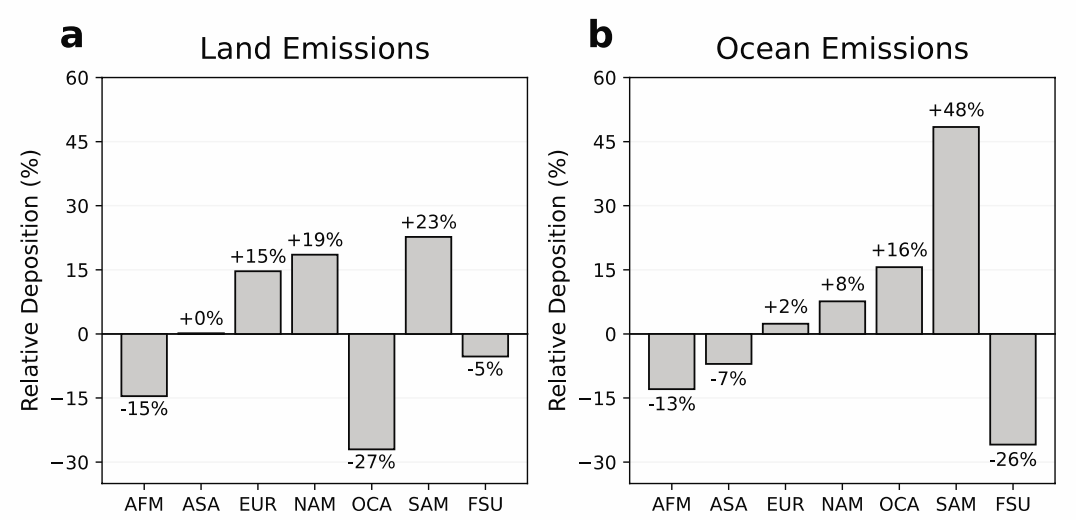

Figure 6. Regional differences in area-normalized atmospheric Hg deposition from natural and legacy sources. Bars represent differences in areal deposition rates between individual receptor regions and the average over land. Positive values mean that receptor regions receive greater deposition per unit area than average, and negative values mean that receptor regions receive less deposition than average. Individual panels show trends in deposition resulting from emissions from the terrestrial biosphere (**a**) and from the ocean (**b**). Receptor regions are Africa and the Middle East (AFM), Asia (ASA), Europe (EUR), North America (NAM), Oceania (OCA), South America (SAM), and the Former Soviet Union (FSU).

Globally averaged seawater Hg concentrations in the upper ocean (0-1500 m) are projected to increase over the coming decades across all scenarios in this study. The Hg reservoir in the upper ocean peaks at 142 to 151 Gg between 2037 (SSP1-2.6) and 2081 (SSP5-8.5) (Fig. S4). Near-term increases in upper ocean Hg concentrations are driven by future rather than historical emissions. Simulated seawater Hg concentrations begin declining in 2015 under a scenario with no future primary anthropogenic Hg releases (Fig. S4). By the end of the 21st century, upper ocean Hg concentrations are projected to be 15% lower than 2010 under SSP1-2.6 and are 11% higher than 2010 under SSP5-8.5.

4 Conclusions

The SSP scenarios evaluated in this work result in a greater than two-fold difference in cumulative anthropogenic Hg emissions between 2010 and 2300. Cumulative anthropogenic emissions to air and releases to land and water between 2010 and 2300 range from 710 Gg under the low-bound scenario (SSP1-2.6) to 1710 Gg under the upper-bound scenario (SSP5-8.5). These future releases are comparable to all-time historical anthropogenic emissions of 1540 Gg (80% CI: 1060 – 2800 Gg) (Streets et al., 2019a).

Transition of the energy sector away from coal combustion is the largest determinant of differences among scenarios, with lower bound and mid-range scenarios (SSPs 1-2.6, 2-4.5, 5-3.4) all exhibiting similar cumulative emissions due to declining coal usage. By contrast, industrial Hg mining and ASGM releases are projected to grow in relative importance in the future. These results imply that under the most stringent climate policies, the largest sources of Hg and CO_2 are likely to become more distinct from one another.

Numerous factors may affect regional Hg deposition patterns in the future. For most regions, reducing primary anthropogenic Hg emissions remains the most effective way to reduce deposition, since 55 – 71% of Hg^{II} emissions redeposit to the region of origin, compared to 5 – 13% for Hg^{0} (Fig. S5). However, the scenario-based trajectories described in this work indicate that anthropogenic Hg^{II} emissions to air will decline more slowly than Hg^{0}, causing Hg^{II} to grow as a fraction of total anthropogenic Hg emissions to air. As the speciation of anthropogenic Hg emissions shifts towards lower fractions of Hg^{0}, a greater proportion of regional emissions will redeposit to the region of origin. Across all regions, the fraction of self-sourced atmospheric Hg deposition is projected to increase from 33% in 2010 to 35% – 45% in 2100 (Fig. S1).

Regional atmospheric Hg deposition patterns over the next century reflect trends in the magnitude and spatial distribution of primary anthropogenic emissions as well as re-emissions from the land and ocean. In regions where anthropogenic Hg emissions reductions are projected to occur, total Hg deposition is expected to decrease, even during periods where global deposition is increasing. This means that domestic policies have significant leverage on domestic Hg deposition (e.g., Dai et al., 2023). However, greater reductions in anthropogenic emissions are accompanied by larger declines in emissions from the land and ocean. Under SSP1-2.6, 28% of the reduction in atmospheric deposition from 2010 to 2100 was the result of declines in legacy emissions. As a result, globally-coordinated efforts to reduce near-term anthropogenic Hg emissions will produce amplified benefits in terms of long-term declines in atmospheric deposition (e.g., Angot et al., 2018).

Acknowledgments

Financial support for this work was provided by the U.S. National Science Foundation (award numbers 2210173 and 2108452). The authors declare no competing financial interest. We thank Zig Klimont of IIASA for providing the detailed activity and emissions datasets for the SSPs used in this work.

Open Research

Mercury emission files, code and model output are available in an OSF repository (peer review link provided with submission). The version of GEOS-Chem used in this study is available from (https://doi.org/10.5281/zenodo.3784796).

References

Alexander, B., & Mickley, L. J. (2015). Paleo-Perspectives on Potential Future Changes in the Oxidative Capacity of the Atmosphere Due to Climate Change and Anthropogenic Emissions. *Current Pollution Reports*, *1*(2), 57–69. https://doi.org/10.1007/s40726-015-0006-0

Amos, H. M., Jacob, D. J., Streets, D. G., & Sunderland, E. M. (2013). Legacy impacts of all-time anthropogenic emissions on the global mercury cycle. *Global Biogeochemical Cycles*, *27*(2), 410–421. https://doi.org/10.1002/gbc.20040

Amos, H. M., Jacob, D. J., Kocman, D., Horowitz, H. M., Zhang, Y., Dutkiewicz, S., et al. (2014). Global Biogeochemical Implications of Mercury Discharges from Rivers and Sediment Burial. *Environmental Science & Technology*, *48*(16), 9514–9522. https://doi.org/10.1021/es502134t

Angot, H., Hoffman, N., Giang, A., Thackray, C. P., Hendricks, A. N., Urban, N. R., & Selin, N. E. (2018). Global and Local Impacts of Delayed Mercury Mitigation Efforts. *Environmental Science and Technology*, *52*(22), 12968–12977. https://doi.org/10.1021/acs.est.8b04542

Basu, N., Bastiansz, A., Dórea, J. G., Fujimura, M., Horvat, M., Shroff, E., et al. (2023). Our evolved understanding of the human health risks of mercury. *Ambio*, *52*(5), 877–896. https://doi.org/10.1007/s13280-023-01831-6

Corbitt, E. S., Jacob, D. J., Holmes, C. D., Streets, D. G., & Sunderland, E. M. (2011). Global source-receptor relationships for mercury deposition under present-day and 2050 emissions scenarios. *Environmental Science and Technology*, *45*(24), 10477–10484. https://doi.org/10.1021/es202496y

Dai, M. Q., Geyman, B. M., Hu, X. C., Thackray, C. P., & Sunderland, E. M. (2023). Sociodemographic Disparities in Mercury Exposure from United States Coal-Fired Power Plants. *Environmental Science & Technology Letters*, *10*(7), 589–595. https://doi.org/10.1021/acs.estlett.3c00216

Dellink, R., Chateau, J., Lanzi, E., & Magné, B. (2017). Long-term economic growth projections in the Shared Socioeconomic Pathways. *Global Environmental Change*, *42*, 200–214. https://doi.org/10.1016/j.gloenvcha.2015.06.004

Fricko, O., Havlik, P., Rogelj, J., Klimont, Z., Gusti, M., Johnson, N., et al. (2017). The marker quantification of the Shared Socioeconomic Pathway 2: A middle-of-the-road scenario for the 21st century. *Global Environmental Change*, *42*, 251–267. https://doi.org/10.1016/j.gloenvcha.2016.06.004

Gelaro, R., McCarty, W., Suárez, M. J., Todling, R., Molod, A., Takacs, L., et al. (2017). The modern-era retrospective analysis for research and applications, version 2 (MERRA-2). *Journal of Climate*, *30*(14), 5419–5454. https://doi.org/10.1175/JCLI-D-16-0758.1

Geyman, B. M., Thackray, C. P., Jacob, D. J., & Sunderland, E. M. (2023). Impacts of Volcanic Emissions on the Global Biogeochemical Mercury Cycle: Insights from Satellite Observations and Chemical Transport Modeling. *Geophysical Research Letters*, *50*, e2023GRL104667. https://doi.org/10.1029/2023GL104667

Gidden, M. J., Riahi, K., Smith, S. J., Fujimori, S., Luderer, G., Kriegler, E., et al. (2019). Global emissions pathways under different socioeconomic scenarios for use in CMIP6: a dataset of harmonized emissions trajectories through the end of the century. *Geoscientific Model Development*, *12*(4), 1443–1475. https://doi.org/10.5194/gmd-12-1443-2019

Guerrero, S., & Schneider, L. (2023). The global roots of pre-1900 legacy mercury. *Proceedings of the National Academy of Sciences*, *120*(31), e2304059120. https://doi.org/10.1073/pnas.2304059120

Horowitz, H M, Jacob, D. J., Zhang, Y., Dibble, T. S., Slemr, F., Amos, H. M., et al. (2017). A new mechanism for atmospheric mercury redox chemistry: implications for the global mercury budget. *Atmos. Chem. Phys.*, *17*(10), 6353–6371. https://doi.org/10.5194/acp-17-6353-2017

Horowitz, Hannah M., Jacob, D. J., Amos, H. M., Streets, D. G., & Sunderland, E. M. (2014). Historical Mercury Releases from Commercial Products: Global Environmental Implications. *Environmental Science & Technology*, *48*(17), 10242–10250. https://doi.org/10.1021/es501337j

Intergovernmental Panel on Climate Change (IPCC). (2023). Summary for Policymakers. In *Climate Change 2021 – The Physical Science Basis: Working Group I Contribution to the Sixth Assessment Report of the*

Intergovernmental Panel on Climate Change (pp. 3–32). Cambridge: Cambridge University Press. https://doi.org/10.1017/9781009157896.001

Jiang, L., & O'Neill, B. C. (2017). Global urbanization projections for the Shared Socioeconomic Pathways. *Global Environmental Change*, *42*, 193–199. https://doi.org/10.1016/j.gloenvcha.2015.03.008

Kc, S., & Lutz, W. (2017). The human core of the shared socioeconomic pathways: Population scenarios by age, sex and level of education for all countries to 2100. *Global Environmental Change*, *42*, 181–192. https://doi.org/10.1016/j.gloenvcha.2014.06.004

Kocman, D., Wilson, S., Amos, H., Telmer, K., Steenhuisen, F., Sunderland, E., et al. (2017). Toward an Assessment of the Global Inventory of Present-Day Mercury Releases to Freshwater Environments. *International Journal of Environmental Research and Public Health*, *14*(2), 138. https://doi.org/10.3390/ijerph14020138

Krabbenhoft, D. P., & Sunderland, E. M. (2013). Global Change and Mercury. *Science*, *341*(6153), 1457–1458. https://doi.org/10.1126/science.1242838

Lund, M. T., Myhre, G., & Samset, B. H. (2019). Anthropogenic aerosol forcing under the Shared Socioeconomic Pathways. *Atmospheric Chemistry and Physics*, *19*(22), 13827–13839. https://doi.org/10.5194/acp-19-13827-2019

Meinshausen, M., Nicholls, Z. R. J., Lewis, J., Gidden, M. J., Vogel, E., Freund, M., et al. (2020). The shared socio-economic pathway (SSP) greenhouse gas concentrations and their extensions to 2500. *Geoscientific Model Development*, *13*(8), 3571–3605. https://doi.org/10.5194/gmd-13-3571-2020

Morfeldt, J., Nijs, W., & Silveira, S. (2015). The impact of climate targets on future steel production - An analysis based on a global energy system model. *Journal of Cleaner Production*, *103*, 469–482. https://doi.org/10.1016/j.jclepro.2014.04.045

Myhre, G., Shindell, D., Bréon, F.-M., Collins, W., Fuglestvedt, J., Huang, J., et al. (2013). Anthropogenic and Natural Radiative Forcing. In T. F. Stocker, D. Qin, G.-K. Plattner, M. Tignor, S. K. Allen, J. Boschung, et al. (Eds.), *Climate Change 2013: The Physical Science Basis.Contribution of Working Group I to the Fifth Assessment Report of the Intergovernmental Panel on Climate Change*. Cambridge, United Kingdom and New York, NY, USA: Cambridge University Press.

Nazarenko, L. S., Tausnev, N., Russell, G. L., Rind, D., Miller, R. L., Schmidt, G. A., et al. (2022). Future Climate Change Under SSP Emission Scenarios With GISS-E2.1. *Journal of Advances in Modeling Earth Systems*, *14*(7), e2021MS002871. https://doi.org/10.1029/2021MS002871

Nriagu, J. O. (1994). Mercury pollution from the past mining of gold and silver in the Americas. *Science of The Total Environment*, *149*(3), 167–181. https://doi.org/10.1016/0048-9697(94)90177-5

O'Neill, B. C., Tebaldi, C., van Vuuren, D. P., Eyring, V., Friedlingstein, P., Hurtt, G., et al. (2016). The Scenario Model Intercomparison Project (ScenarioMIP) for CMIP6. *Geoscientific Model Development*, *9*(9), 3461–3482. https://doi.org/10.5194/gmd-9-3461-2016

O'Neill, B. C., Kriegler, E., Ebi, K. L., Kemp-Benedict, E., Riahi, K., Rothman, D. S., et al. (2017). The roads ahead: Narratives for shared socioeconomic pathways describing world futures in the 21st century. *Global Environmental Change*, *42*, 169–180. https://doi.org/10.1016/j.gloenvcha.2015.01.004

Pacyna, J. M., Travnikov, O., Simone, F. D., Hedgecock, I. M., Sundseth, K., Pacyna, E. G., et al. (2016). Current and future levels of mercury atmospheric pollution on a global scale. *Atmospheric Chemistry and Physics*, *16*(19), 12495–12511. https://doi.org/10.5194/acp-16-12495-2016

Rae, J. W. B., Zhang, Y. G., Liu, X., Foster, G. L., Stoll, H. M., & Whiteford, R. D. M. (2021). Atmospheric CO_2 over the Past 66 Million Years from Marine Archives. *Annual Review of Earth and Planetary Sciences*, *49*(1), 609–641. https://doi.org/10.1146/annurev-earth-082420-063026

Rao, S., Klimont, Z., Smith, S. J., Van Dingenen, R., Dentener, F., Bouwman, L., et al. (2017). Future air pollution in the Shared Socio-economic Pathways. *Global Environmental Change*, *42*, 346–358. https://doi.org/10.1016/j.gloenvcha.2016.05.012

659 Riahi, K., van Vuuren, D. P., Kriegler, E., Edmonds, J., O'Neill, B. C., Fujimori, S., et al. (2017). The Shared
660 Socioeconomic Pathways and their energy, land use, and greenhouse gas emissions implications: An
661 overview. *Global Environmental Change*, *42*, 153–168. https://doi.org/10.1016/j.gloenvcha.2016.05.009
662 Schaefer, K., Elshorbany, Y., Jafarov, E., Schuster, P. F., Striegl, R. G., Wickland, K. P., & Sunderland, E. M.
663 (2020). Potential impacts of mercury released from thawing permafrost. *Nature Communications*, *11*(1),
664 4650. https://doi.org/10.1038/s41467-020-18398-5
665 Schartup, A. T., Thackray, C. P., Qureshi, A., Dassuncao, C., Gillespie, K., Hanke, A., & Sunderland, E. M. (2019).
666 Climate change and overfishing increase neurotoxicant in marine predators. *Nature*, *572*(7771), 648–650.
667 https://doi.org/10.1038/s41586-019-1468-9
668 Shah, V., Jacob, D. J., Thackray, C. P., Wang, X., Sunderland, E. M., Dibble, T. S., et al. (2021). Improved
669 Mechanistic Model of the Atmospheric Redox Chemistry of Mercury. *Environmental Science &*
670 *Technology*, acs.est.1c03160. https://doi.org/10.1021/acs.est.1c03160
671 Steenhuisen, F., & Wilson, S. J. (2019). Development and application of an updated geospatial distribution model
672 for gridding 2015 global mercury emissions. *Atmospheric Environment*, *211*(December 2018), 138–150.
673 https://doi.org/10.1016/j.atmosenv.2019.05.003
674 Streets, D. G., Zhang, Q., & Wu, Y. (2009). Projections of global mercury emissions in 2050. *Environmental*
675 *Science and Technology*, *43*(8), 2983–2988. https://doi.org/10.1021/es802474j
676 Streets, D. G., Devane, M. K., Lu, Z., Bond, T. C., Sunderland, E. M., & Jacob, D. J. (2011). All-time releases of
677 mercury to the atmosphere from human activities. *Environmental Science and Technology*, *45*(24), 10485–
678 10491. https://doi.org/10.1021/es202765m
679 Streets, D. G., Horowitz, H. M., Jacob, D. J., Lu, Z., Levin, L., ter Schure, A. F. H., & Sunderland, E. M. (2017).
680 Total Mercury Released to the Environment by Human Activities. *Environmental Science & Technology*,
681 *51*(11), 5969–5977. https://doi.org/10.1021/acs.est.7b00451
682 Streets, D. G., Horowitz, H. M., Lu, Z., Levin, L., Thackray, C. P., & Sunderland, E. M. (2019a). Five hundred
683 years of anthropogenic mercury: spatial and temporal release profiles*. *Environmental Research Letters*,
684 *14*(8), 084004. https://doi.org/10.1088/1748-9326/ab281f
685 Streets, D. G., Horowitz, H. M., Lu, Z., Levin, L., Thackray, C. P., & Sunderland, E. M. (2019b). Global and
686 regional trends in mercury emissions and concentrations, 2010–2015. *Atmospheric Environment*,
687 *201*(December 2018), 417–427. https://doi.org/10.1016/j.atmosenv.2018.12.031
688 Sverdrup, H., Koca, D., & Granath, C. (2012). Modelling the gold market, explaining the past and assessing the
689 physical and economical sustainability of future scenarios. *Proceedings of the 30th International*
690 *Conference of the System Dynamics Society*, 1–23.
691 Sverdrup, H. U., & Olafsdottir, A. H. (2020). System Dynamics Modelling of the Global Extraction, Supply, Price,
692 Reserves, Resources and Environmental Losses of Mercury. *Water, Air, and Soil Pollution*, *231*(8), 1–22.
693 https://doi.org/10.1007/s11270-020-04757-x
694 Sverdrup, H. U., Olafsdottir, A. H., & Ragnarsdottir, K. V. (2019). On the long-term sustainability of copper, zinc
695 and lead supply, using a system dynamics model. *Resources, Conservation and Recycling: X*, *4*, 100007.
696 https://doi.org/10.1016/j.rcrx.2019.100007
697 Turnock, S. T., Allen, R. J., Andrews, M., Bauer, S. E., Deushi, M., Emmons, L., et al. (2020). Historical and future
698 changes in air pollutants from CMIP6 models. *Atmospheric Chemistry and Physics*, *20*(23), 14547–14579.
699 https://doi.org/10.5194/acp-20-14547-2020
700 Watari, T., Nansai, K., Giurco, D., Nakajima, K., McLellan, B., & Helbig, C. (2020). Global Metal Use Targets in
701 Line with Climate Goals. *Environmental Science & Technology*, *54*(19), 12476–12483.
702 https://doi.org/10.1021/acs.est.0c02471
703 Watari, T., Nansai, K., & Nakajima, K. (2021). Major metals demand, supply, and environmental impacts to 2100:
704 A critical review. *Resources, Conservation and Recycling*, *164*, 105107.
705 https://doi.org/10.1016/j.resconrec.2020.105107
706 Wu, X., Fu, X., Zhang, H., Tang, K., Wang, X., Zhang, H., et al. (2023). Changes in Atmospheric Gaseous
707 Elemental Mercury Concentrations and Isotopic Compositions at Mt. Changbai During 2015–2021 and Mt.

Ailao During 2017–2021 in China. *Journal of Geophysical Research: Atmospheres*, *128*(10), e2022JD037749. https://doi.org/10.1029/2022JD037749

Yang, Y., Meng, L., Yanai, R. D., Montesdeoca, M., Templer, P. H., Asbjornsen, H., et al. (2019). Climate change may alter mercury fluxes in northern hardwood forests. *Biogeochemistry*, *146*(1), 1–16. https://doi.org/10.1007/s10533-019-00605-1

Zhang, C. Y., Han, R., Yu, B., & Wei, Y. M. (2018). Accounting process-related CO2 emissions from global cement production under Shared Socioeconomic Pathways. *Journal of Cleaner Production*, *184*, 451–465. https://doi.org/10.1016/j.jclepro.2018.02.284

Zhang, Y., Zhang, L., Cao, S., Liu, X., Jin, J., & Zhao, Y. (2023). Improved Anthropogenic Mercury Emission Inventories for China from 1980 to 2020: Toward More Accurate Effectiveness Evaluation for the Minamata Convention. *Environmental Science & Technology*, *57*(23), 8660–8670. https://doi.org/10.1021/acs.est.3c01065

Zolkos, S., Zhulidov, A. V., Gurtovaya, T. Yu., Gordeev, V. V., Berdnikov, S., Pavlova, N., et al. (2022). Multidecadal declines in particulate mercury and sediment export from Russian rivers in the pan-Arctic basin. *Proceedings of the National Academy of Sciences*, *119*(14). https://doi.org/10.1073/pnas.2119857119